

ARTICLE

OPEN

Famines and likelihood of consecutive megadroughts in India

Vimal Mishra^{1,2}✉ and Saran Aadhar¹

Consecutive failures in the summer monsoon rainfall led to widespread and severe droughts with profound implications for agricultural activities in India. However, the likelihood of successive megadroughts in India's past and future climate remain poorly understood. Using Palmer Drought Severity Index (PDSI) from the Monsoon Asia Drought Atlas (MADA), we show that the major famines that affected millions of people during 1200–2018 were linked with summer monsoon droughts. Four megadroughts covering more than 40% of the country occurred for two consecutive summer monsoon seasons during 1200–2018. The most recent and severe megadrought occurred in 2002–2003. Simulations from the Community Earth System Model (CESM) for the last millennium (850–2005) ensemble (LME) show that the likelihood of two and three-year consecutive megadroughts during the summer monsoon is about 0.7 and 0.3 events per 100 years, respectively. Large ensemble simulations from CESM (CESM-LE) show a decline in the frequency of megadroughts in the future. Summer monsoon megadroughts are strongly associated with the warm sea surface temperature (SST) anomalies over the Pacific Ocean in the past and future climate. Substantial warming under the projected future climate can cause megadroughts under near-normal precipitation during the summer monsoon season. Despite the projected decline in the likelihood of the summer monsoon megadroughts under the warming climate, megadroughts in the future can have considerable implications for India's food production and water availability.

npj Climate and Atmospheric Science (2021)4:59; <https://doi.org/10.1038/s41612-021-00219-1>

INTRODUCTION

Indian summer monsoon (June–September) accounts for more than 80% of the total annual rainfall¹. Rainfall during the summer monsoon plays a vital role in the Indian economy^{2,3}. The Indian summer monsoon has a year-to-year variability of about 10% of its long-term mean^{1,2}. A rainfall deficit of more than 10% is considered a drought, while rainfall of more than 10% of the long-term mean is termed surplus². A deficit of 19–21% in rainfall in 2002 caused a drought that resulted in an estimated loss of billions of dollars, which was about 1% in the Gross Domestic Product (GDP) of India⁴. From 1901 through 2010, 17% of the total years experienced drought during the summer monsoon season. Characteristics and the occurrence of droughts during the summer monsoon season are well studied^{1,4–8}. About 18 meteorological droughts occurred in India during the 1870–2018 period⁷. The severe meteorological and hydrological droughts occurred in 1876, 1899, 1918, 1965, and 2000⁷. While droughts due to summer monsoon failure have implications, consecutive droughts disrupt India's socio-economic well-being. For instance, the drought of 2015–2018 caused groundwater depletion and affected about one-fourth of the total Indian population^{7,8}. Similarly, the drought of 1875–1876 caused the great famine and affected millions of people in India^{9,10}.

The year-to-year variability of the Indian summer monsoon is influenced by El Niño Southern Oscillation (ENSO)^{11–16}. Warm sea surface temperature (SST) anomalies over the Pacific Ocean are negatively related to the Indian summer monsoon rainfall (ISMR). The negative relationship between summer monsoon rainfall and SST anomalies is the strongest over the eastern Pacific region¹⁵. The physical mechanism of the linkage between ENSO and the Indian summer monsoon is associated with atmospheric circulation and ENSO-induced SST variability¹⁷. The coupled atmospheric and oceanic variability modify Walker circulation and connect the rising motion over the central-eastern Pacific during a warm phase

of ENSO with reduced rainfall over India¹⁷. While ENSO is one of the significant drivers of the year-to-year variability of the Indian summer monsoon, other forcings are related to SST patterns over the Indian Ocean, Atlantic Ocean, and other parts of the Pacific Ocean affect ISMR. For instance, Indian Ocean Dipole (IOD) is a dominant mode of coupled ocean-atmospheric variability, influencing summer monsoon^{18–22}. A positive phase of IOD is linked with the above-normal summer monsoon rainfall^{23–25}. Moreover, IOD modulates the teleconnection between ENSO and ISMR^{25,26}. At the decadal time scale, Pacific decadal oscillation (PDO) influences the summer monsoon through a modification of the Walker circulation and adjustment in the Indian ocean Hadley cell^{27,28}. Similarly, at a multidecadal time scale, Atlantic multidecadal oscillation (AMO) influences the summer monsoon^{29,30} through modifying the tropospheric temperature gradient¹⁷.

India has a long history of famines^{31–33}. Famines caused significant mortality due to lack of food availability, resulting from crop failures and other factors⁹. The history of famines in India reported in the scientific literature goes back to 503–443 BC³¹. Famines occurred in a large number in India during the pre-British era. While the number of local/regional famines that affected a small part of the country is considerably higher³¹, India witnessed twenty major famines from 1200 to 1945. Out of these major famines, nine famines were widespread and caused the loss of millions of lives in India. The summer monsoon failures and droughts^{9,31,33} caused a majority of the famines. Agricultural drought due to soil moisture deficit and crop failure resulted in food insecurity, which primarily caused most famines in India during the British Era^{9,10}. For instance, out of six major famines (1873–1874, 1876, 1877, 1896–1897, 1899, and 1943) during 1870–2018, soil moisture drought⁹ was the main reason for the five (1873–74, 1876, 1877, 1896–97, and 1899). On the other hand, summer monsoon failure and drought were not associated with the Bengal famine of 1943; instead, it occurred due to policy

¹Civil Engineering, Indian Institute of Technology (IIT) Gandhinagar, Gandhinagar, India. ²Earth Sciences, Indian Institute of Technology (IIT) Gandhinagar, Gandhinagar, India.
✉ email: vmishra@iitgn.ac.in

failures and conflict^{9,34}. Therefore, understanding major droughts and the causes of their occurrence in the long-term historical record is crucial.

A relatively short observational record of a century and half period does not provide crucial information on the megadroughts that caused famines before the 1870s in India. Long-term paleoclimate reconstructions based on the historical documents and tree ring datasets^{35–39} have been used to examine droughts and famine across the globe^{35–39}. Paleoclimate records over the Indian monsoon region showed that the Indian summer monsoon's year-to-year variability is higher than the estimates based on the observations⁴⁰. Seasonally resolved gridded reconstruction of monsoon failures based on the network of tree ring chronologies can reveal the occurrence of megadroughts over the past millennium³⁵. As the past droughts were the leading cause of most famines that India witnessed^{9,31}, it is crucial to examine the likelihood of the megadroughts and their drivers in the past and future. We identify the two critical research gaps: (i) several famines that occurred before the 1870s and affected millions of people in India; however, their causes and linkage with the monsoon failures are not well understood and (ii) the role of substantial projected warming on the occurrence of megadroughts in India remains unexplored. In consecutive years, a widespread failure of the summer monsoon can cause megadroughts with profound implications for agriculture and water availability. However, estimation of megadrought using a short-term record is challenging due to its low probability of occurrence. To address these gaps, we use Palmer Drought Severity Index (PDSI) based on the Monsoon Asia Drought Atlas (MADA, 1200–2012) and Climate Research Unit (CRU, 2013–2018) to examine the likelihood of megadroughts that occurred for the 2 and 3 consecutive years during 1200–2018. Also, we use long-term simulations from the Community Earth System Model (CESM) to estimate the likelihood of megadroughts during the summer monsoon season in India in the last millennium (850–2005) and the projected future climate (2021–2100).

RESULTS

Consecutive megadroughts in India, 1200–2018

We used the PDSI for June–August (JJA) period from MADA^{35,36} (MADA-PDSI hereafter), which is available at 1° spatial resolution for the monsoon Asia domain (see Methods for more details). MADA-PDSI, available for 1200–2012, was extended till 2018 using gridded observations from Climate Research Units (CRU). Since MADA-PDSI for 1990–2012 is based on the CRU datasets, we used CRU observations to construct PDSI for the 2013–2018 period. We identified consecutive megadroughts during two or three summer monsoon seasons using the long-term (1200–2018) record of PDSI. As consecutive summer monsoon failures have considerable implications for water availability and agriculture^{10,41}, megadroughts were identified if these affected more than 40% of the country, and all-India averaged PDSI was less than −1.5 for 2/3 consecutive years. We selected only widespread droughts to reduce uncertainty in MADA-PDSI^{35,42,43}, which might be associated with localized droughts. We identified six megadroughts that occurred consecutively for 2 or 3 years during the entire record of 1200–2018 (Supplementary Table 1). Four megadroughts that lasted for 2 consecutive years (JJA) were 1256–1257, 1423–1424, 1702–1703, and 2002–2003 (Supplementary Table 1). On the other hand, only two (1431–1433 and 1721–1723) megadroughts remained consecutively for 3 years. The mean area for five out of six megadroughts was more than 50%, while the maximum area affected by megadrought ranged from 48 to 72% of the country (Supplementary Table 1). We ranked these megadroughts based on the overall severity score that combines intensity, duration, and area under drought⁷. Based on the overall severity score, 1721–1723 was the most severe drought during the monsoon season in India. The peak intensity of the megadroughts occurred in 1721, 1431, 2002, 1257, 1424, and 1703 with the affected area of 72%, 52.5%, 65%, 51.5%, 52%, and 48% of the country, respectively (Fig. 1). 2002–2003 was the only megadrought that occurred during the recent decades, which affected more than 65% of the country (Fig. 1). The 2002 drought was primarily caused by a rainfall deficit (~51%) in the month of July^{44,45}.

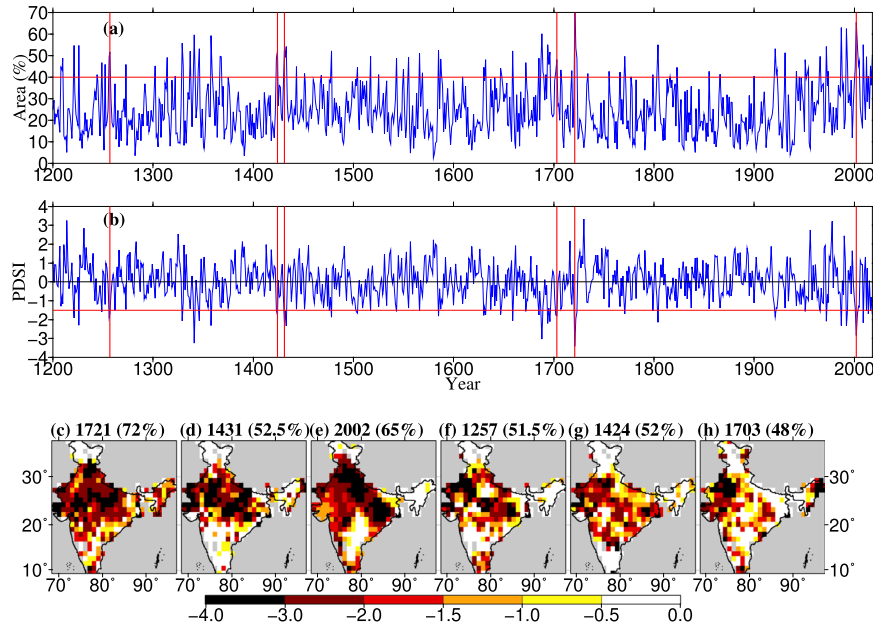


Fig. 1 Occurrence of megadroughts during the monsoon (June–August) in India, 1200–2018. **a** Area (%) under drought estimated using Palmer Drought Severity Index (PDSI) less than −1, **b** summer monsoon PDSI during 1200–2018, **c–h** years that experienced peak drought during the six megadroughts during 1200–2018. Values in parenthesis in **(c–h)** show the area (%) under drought for the peak intensity for the megadroughts. Vertical pink lines in **(a, b)** indicate the occurrence of megadroughts. The six megadroughts occurred in 1256–1257, 1423–1424, 1431–1433, 1702–1703, 1721–1723, and 2002–2003.

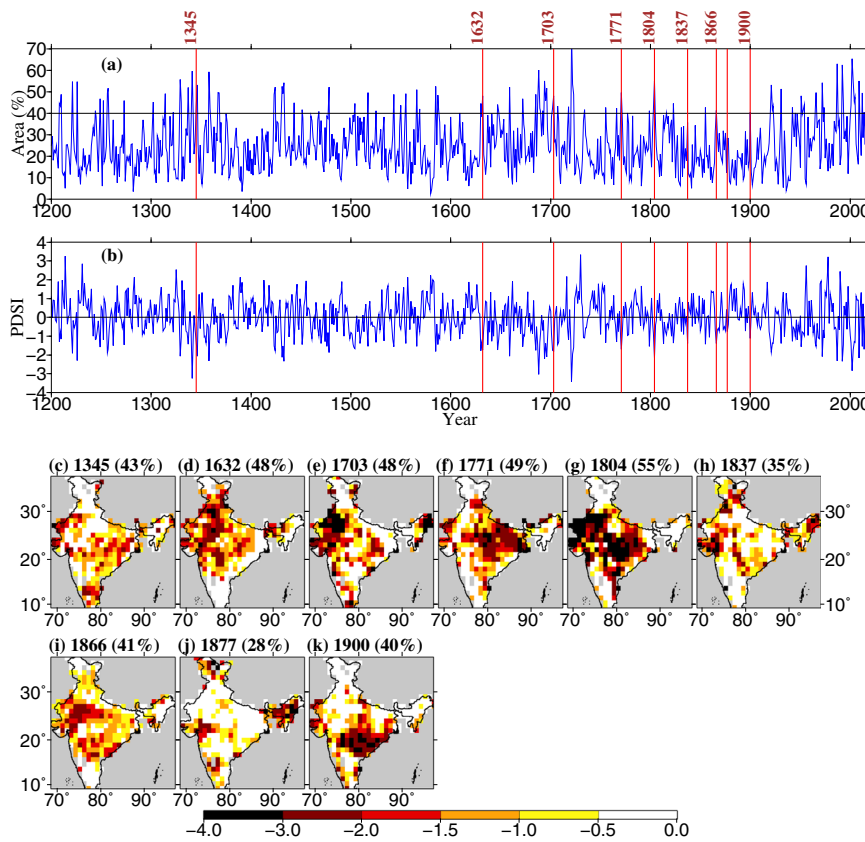


Fig. 2 Major famines caused by drought in India during 1200–2018. **a** Area (%) under drought estimated using Palmer Drought Severity Index (PDSI) less than -1 , **b** summer monsoon PDSI during 1200–2018, **c–h** years that experienced peak drought during the nine major famines that occurred in the 1200–2018 period. Values in parenthesis in **c–h** show the area (%) under drought for the peak intensity. Vertical pink lines in **(a, b)** indicate the occurrence of the nine major famines caused by the summer monsoon failures during 1200–2018.

Reconstruction of famines caused by droughts

The spatiotemporal information from the MADA on the summer monsoon failures provides a long-term context of droughts that occurred during the past over Monsoon Asia⁴⁶. Famines in India were instigated by droughts and caused the death of millions of people⁹. Instrumental meteorological record in India does not go beyond 1870^{9,10}, which hampers our understanding of the underlined causes of the famines before 1870. Nine major famines caused by droughts were identified from the database developed by Walford (1878)³¹ and other sources⁴⁷ [Supplementary Table 2, Fig. 2]. These nine major famines occurred during 1344–1345, 1630–1632, 1702–1704, 1769–1771, 1802–1804, 1837–1838, 1866, 1877, and 1899–1900^{31,47} [Supplementary Table 1]. The last famine of 1899–1900 was identified based on the Imperial Gazetteer of India (1907)⁴⁸. As droughts and the summer monsoon failures⁹ caused most famines in the post-1870 period, we used MADA-PDSI to identify the droughts and affected regions during each famine (Fig. 2).

India experienced a famine that was extended to the entire country during 1344–1345^{31,49}. The famine of 1344–1345 severely affected the Deccan part of India³¹. The famine was so acute that the Mughal emperor could not procure necessary items for his household^{31,49}. MADA-PDSI captured the 1345 drought, which affected about 43% of the country (Supplementary Table 2, Fig. 2). The subsequent major famine occurred in 1631. Walford (1878)³¹ reported that a famine was caused by drought and war in 1631. Moreover, the great drought that occurred in 1631 affected a large part of India and Asia³¹. The 1630–1632 famine is also known as the Deccan famine, which affected Deccan Plateau, Khandesh, and Gujarat⁵⁰. The famine resulted from staple crops' failure for 3 consecutive years and led to intense hunger, diseases,

and migration. 1630–1632 was one of India's worst famines during the Mughal Empire^{51,52}. We find that MADA-PDSI captured the drought during 1630–1632 peaked in 1632 (Fig. 2). The 1630–1632 drought affected about half of the country and was centered in India's central and northwestern parts (Fig. 2). The other major famine in India occurred during 1702–1704³¹. The famine affected western India's parts and was mainly centered in Thar and Parkar (now in Pakistan) districts³¹. The famine was caused by drought killed more than two million people⁵¹. We find that 1702–1703 is also captured using MADA-PDSI as the megadrought of the 2 consecutive years (Fig. 2, Supplementary Table 1). The drought pattern exhibited by MADA-PDSI shows that the 1703 drought was more intense in western India³¹ than in other regions [Fig. 2].

India experienced another great famine during 1769–1773^{31,53}, also known as the Great Bengal Famine of 1770. The total reported deaths due to the famine ranged between 2 and 10 million⁵³, with an approximate reduction of 7–33% in the total population of Bengal⁵⁴. Based on the MADA-PDSI, we find that the 1769–1771 drought severely affected northern India and the Gangetic Plain, which peaked in 1771, affecting about half of the country (Supplementary Table 2; Fig. 2). The subsequent major famine in India occurred during 1802–1804³¹. The drought of 1802–1804 peaked in 1804 and affected about 55% of the country, which was well captured by MADA-PDSI (Fig. 2, Supplementary Table 2). India witnessed another notable famine in 1837–1838, which affected northwest provinces³¹. The 1837–38 famine is also known as the Agra famine of 1837–1838, which involved a large part of Uttar Pradesh. We find that the MADA-PDSI captured the drought during 1837, which affected about 35% of the country (Fig. 2). India witnessed a major famine in 1866, which is also known as the Orissa famine of 1866. The famine affected Bengal, Orissa, and

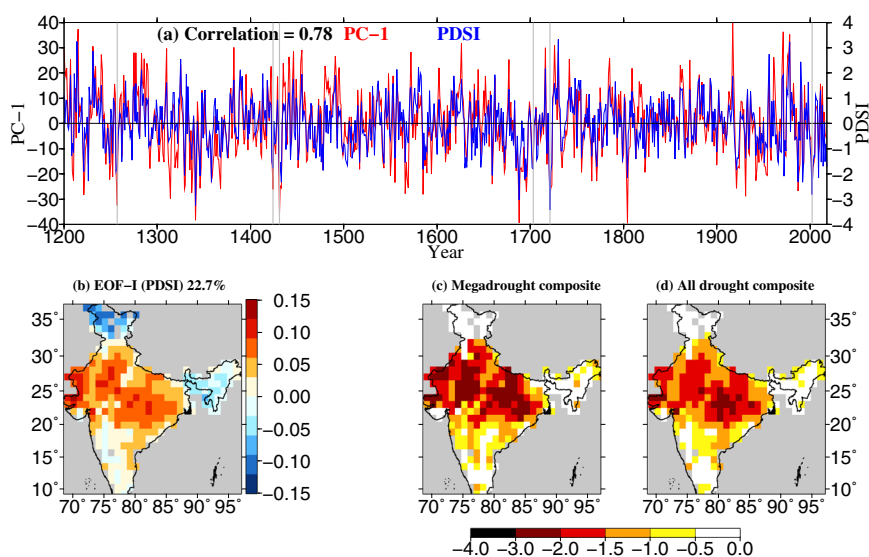


Fig. 3 Dominant mode of variability of summer monsoon droughts during 1200–2018. **a**, Correlation between a principal component of the leading mode (PC-1) obtained from the empirical orthogonal function (EOF) analysis of PDSI and original PDSI time series; **b**, leading mode of EOF analysis (EOF-1); **c**, composite of the six megadroughts that occurred during 1200–2018, and **d**, composites of all the droughts with all-India averaged PDSI less than -1.5 and area more than 40% occurred during the entire period.

Bihar's lower provinces, which caused the death of one and half million people³¹. The famine was caused by the failure of the summer monsoon rainfall during the late season⁴⁸. The famine had an unprecedented influence on the demography as about one-third of the total population of Orissa died⁵⁵. MADA-PDSI captured the drought reasonably well (Fig. 2, Supplementary Table 2).

Madras's Presidency witnessed one of the most extended famines in 1877 that caused the death of more than 10 million people. MADA-PDSI captured the drought in Bombay (now in Maharashtra), but the drought intensity is weaker in south India than reported in the previous studies^{9,10}. As MADA-PDSI covers only JJA period, it does not account for the summer monsoon variability during the late monsoon season (September). Also, MADA-PDSI does not account for the rainfall variability during the northeast monsoon (October–December), affecting southern India⁵⁶. The last famine of the 19th century occurred in 1899–1900, which affected central and western parts of India. The famine caused deaths of about 1–4.5 million people and affected central India, Hyderabad, and Rajputana agency⁴⁷. MADA-PDSI captured drought in some famine-affected regions (Fig. 2), which covered about 40% of the country in 1900 (Supplementary Table 2, Fig. 2). Overall, the famines caused by the summer monsoon droughts in the previously reported studies are captured by MADA-PDSI, which provides us with a basis to examine the occurrence and likelihood of the consecutive megadroughts in India.

The leading mode of variability of droughts

Next, we compared MADA-PDSI based on paleoclimate records against the PDSI estimated using gridded observations from CRU for a common period of 1901–1989 (Supplementary Fig. 1). PDSI from MADA v2 for the 1200–1989 period is based on the paleoclimate reconstruction^{35,36} while the estimates after 1989 are based on the CRU observations⁵⁷. The reconstructed PDSI from the paleoclimate records compares well (correlation = 0.63, p -value < 0.05) with the CRU-based PDSI (Supplementary Fig. 1). All the major droughts during the 1901–1989 period were well captured by the paleoclimate-based reconstructed PDSI (Supplementary Fig. 1b). Comparison of PDSI based on paleoclimate record and CRU data further demonstrates that reconstruction

based on a network of tree-ring chronologies provides valuable information on droughts during the summer monsoon over India³⁵. Identifying droughts that caused famines provides confidence to use the MADA-PDSI to examine the megadroughts' variability and occurrence in India.

We used empirical orthogonal function (EOF) analysis to examine the dominant mode of variability in MADA-PDSI for the entire record of 1200–2018 (Fig. 3). The principal component of the leading mode (PC-1) of MADA-PDSI is well correlated ($r = 0.78$, p -value < 0.05) with PDSI. Also, all the six megadroughts were well captured by the PC-1 (Fig. 3a). The leading mode of variability in MADA-PDSI explains about 22.7% of the total variance (Fig. 3b). The spatial pattern of EOF-1 of MADA-PDSI shows positive loadings in most of India except for the southern peninsula, northeastern regions, and Jammu and Kashmir (Fig. 3b). Since the negative values of PC-1 co-occur with the megadroughts (PDSI), leading EOF mode (EOF-1) of MADA-PDSI indicates that most of the megadroughts were centered in the central and northern parts of the country (Fig. 3b). We constructed the composite of MADA-PDSI for the six megadroughts (Supplementary Table 1), which exhibits a similar spatial pattern obtained from EOF-1 (Fig. 3c). We also identified all the droughts during the summer monsoon (JJA) with PDSI less than -1.5 and covered 40% or more of the country during 1200–2018. A total of fifty such droughts occurred in the record of 819 years (1200–2018). MADA-PDSI composite of all the 50 droughts displayed a somewhat identical spatial pattern that was reflected in EOF-1 and the 6 megadroughts. Therefore, the leading mode of drought variability obtained from the MADA PDSI shows that drought-affected northern and central India more than the other parts of the country (Fig. 3).

We used maximum covariance analysis (MCA)^{58,59} to obtain the leading mode of coupled variability between the summer monsoon precipitation and SST anomalies (Fig. 4). SST anomalies over the Pacific Ocean are negatively associated with the summer (JJA) monsoon precipitation over India during the observed record of 1901–2018, for which observed SST is available (Fig. 4a, b). The leading mode of coupled variability obtained from the MCA explains about 70% of total squared covariance and corresponding principal components (PC-1) are strongly correlated ($r = 0.53$, p -value < 0.05). The long-term record (1200–2018) of MADA-PDSI showed that the megadrought of 2002–2003 was the most severe

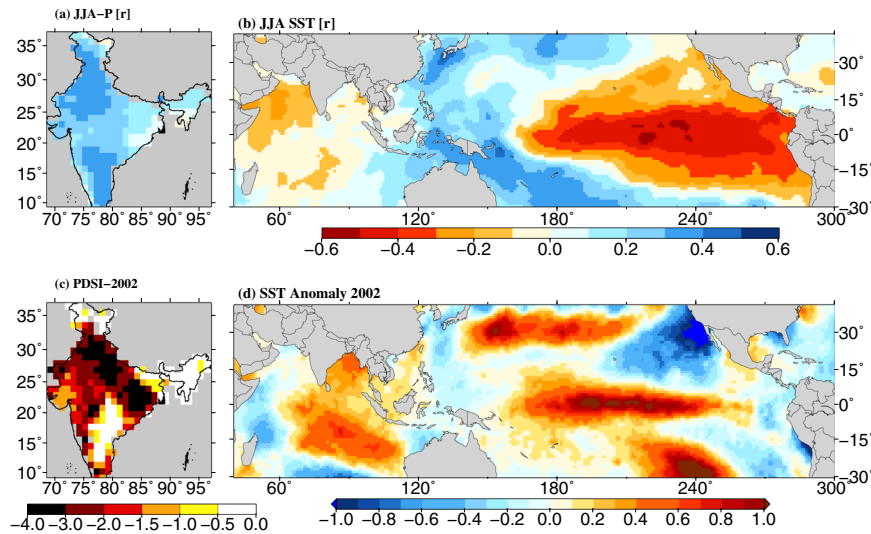


Fig. 4 The role of sea-surface temperature variability during the megadrought of 2002. **a, b** Heterogeneous correlation (r) patterns of coupled variability between the summer monsoon (June–August) precipitation and sea surface temperature (SST) obtained from the first leading mode of maximum covariance analysis (MCA). MCA was conducted on JJA precipitation and SST anomalies during 1901–2018. **c** Palmer drought severity index (PDSI) for the megadrought of 2002. **d** sea surface temperature (SST) anomaly during the summer monsoon of 2002. Precipitation and SST were obtained from the climate research unit (CRU) and Hadley Centre (HadSST), respectively.

drought in the two consecutive monsoon seasons in the entire record of 1200–2018 (Supplemental Table S1, Fig. 4c). We, therefore, examined the spatial variability in MADA-PDSI during the summer monsoon (JJA) of 2002 and associated SST anomaly (Fig. 4d, Supplementary Fig. 2). A majority of north India was affected by drought during 2002 (Fig. 4c). For instance, drought was severe over the Indo-Gangetic Plain and northwestern India.

Based on the Hadley Center's (HadSST) observations, SST exhibits warmer anomaly over the Pacific and Indian Ocean (Fig. 4d, Supplementary Fig. 2). Warmer SST anomaly over the Pacific during the summer monsoon of 2002 indicates the presence of El Nino⁴⁴. El Nino and warmer SST over the central equatorial Pacific are more strongly related to India's monsoon failures than the warmer SST anomaly over the eastern equatorial Pacific⁶⁰. In addition to El-Nino, IOD also influences the summer monsoon rainfall, a dominant mode of coupled variability between the ocean and atmosphere^{18–22}. The positive dipole mode index (DMI) is linked with above normal ISMR^{23–25} and modulates the teleconnection between El Nino and summer monsoon rainfall^{25,26}. For instance, concurrent El Nino and positive DMI reduces the effect of El Nino on the Indian summer monsoon and strengthens the monsoon rainfall²⁵. We find a negative DMI and warm SST anomaly over the Indian Ocean during the summer monsoon season of 2002 (Fig. 4d, Supplementary Fig. 2). El Nino and negative DMI strengthen the intensity of drought during the year 2002. Moreover, warmer SST anomalies in the Indian Ocean are linked with the drying over the Indo-Gangetic Plain^{13,61}. Land-sea thermal gradient has been declining over South Asia due to higher warming over the Indian Ocean than lesser warming over the land⁶¹. Due to a decrease in land-ocean thermal gradient, Hadley circulation weakens, which results in reduced rainfall over parts of northern India⁶¹. Moreover, warming in the Indian Ocean SST is linked with the troposphere ridge over north India, resulting in a decline in rainfall⁶². PDO and AMO also influence summer monsoon rainfall over India directly or indirectly^{27,63}. We find a negative phase of PDO during the onset of the summer monsoon drought of 2002, which turned to a positive phase during late 2002 and 2003. Droughts during the summer monsoon season can intensify during the El-Nino overlapped with a positive phase PDO²⁷. We find a negative phase of AMO during the summer monsoon of 2002, which

suppresses rainfall over India^{29,30}. Therefore, SST warming in both the Pacific and Indian Oceans affected the 2002 drought in India during the summer monsoon.

We obtained total column rainwater (TCRW) and wind (u and v components) from ERA5 reanalysis to examine the climatological and anomalous features during the 2002 observed drought (Supplementary Fig. 3). Climatological mean patterns show high TCRW over India and the central Pacific Ocean during the summer monsoon. A strong westerly flow signifies the moisture transport from tropospheric winds from the Indian Ocean to the Indian landmass (Supplementary Fig. 3a). During the summer monsoon of 2002, the weakening of westerly winds can be noted over the Indian mainland along with the dry anomaly of TCRW (Supplementary Fig. 3b). Therefore, the decline of westerly moisture transport is associated with the 2002 drought over India, as reported in the previous studies⁴⁴. The 2002 drought was caused by a rainfall deficit of 21.5% during the monsoon, while 56% rainfall deficit occurred during July⁶⁴. Consistent with the SST anomaly patterns over the Pacific and Indian oceans during the summer monsoon of 2002, a negative relationship between MADA-PDSI and SST anomalies (JJA) exhibited the role of ENSO on the summer monsoon failure and droughts over India^{13,61} (Fig. 4a, b). For instance, MADA-PDSI is significantly (P -value < 0.05) correlated with the SST anomalies over the Pacific and Indian Oceans (Fig. 4b). Also, Overall, the long-term MADA-PDSI and observed SST exhibited the role of ENSO on droughts over India as reported in the previous studies^{13,60,61}.

Consecutive megadroughts in the past and future

The occurrence of the consecutive megadroughts during the summer monsoon season over India has profound implications^{1,78}. For instance, consecutive monsoon failures over the Indo-Gangetic Plain during 2014–2015 caused water scarcity and groundwater depletion⁸. Moreover, the drought during 2016–2018 in South India due to the northeastern monsoon's failure resulted in a water crisis over a large region³⁶. As CESM-Last Millennium Ensemble (LME) [CESM-LME hereafter] captures the coupled variability between summer monsoon rainfall and SST reasonably well⁶⁵ (Supplementary Fig. 4), we estimated the occurrence of the consecutive megadroughts using the 12 ensemble members from the CESM-LME. Also, CESM-LME captures

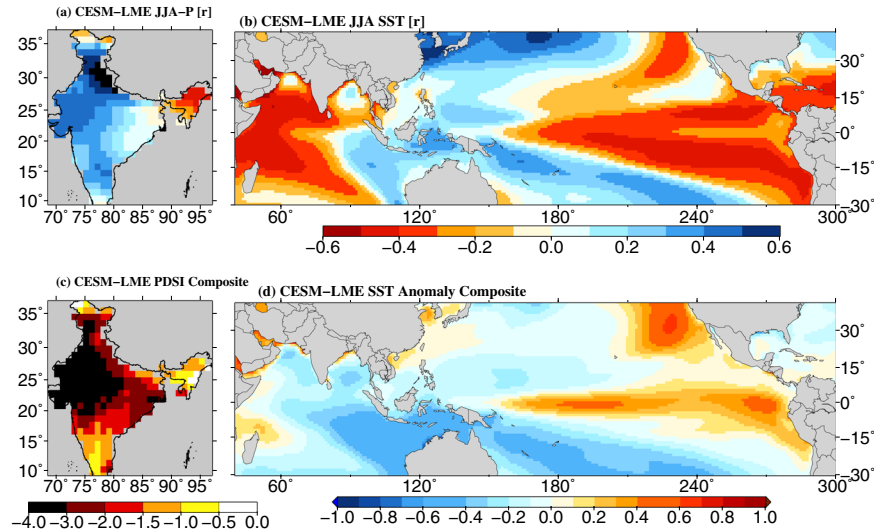


Fig. 5 The role of sea-surface temperature during megadroughts in CESM large millennium ensemble (LME). **a, b** Composite heterogeneous correlation (r) patterns of coupled variability of the summer monsoon precipitation and SST obtained from the first leading mode of maximum covariance analysis (MCA) from the 12 ensemble members of CESM-LME. MCA was conducted on JJA precipitation and SST anomalies using the CESM-LME for each ensemble member for the 850–2005 period. **c** Composite Palmer Drought Severity Index (PDSI) for all the megadroughts that occurred in the 12 ensemble members of CESM-LME. **d** composite sea surface temperature (SST) anomaly during the megadroughts.

the critical feature of the Indian summer monsoon and seasonal cycle of rainfall well (Supplementary Fig. 5).

First, we estimated PDSI for each ensemble member of the CESM-LME, drought characteristics were calculated. Out of the four megadroughts that occurred consecutively for 2 years based on the MADA-PDSI (Supplementary Table 1), the drought of 2002–2003 had the highest overall severity score (274.6), while the drought of 1702–1703 had the lowest overall severity score (160.6). We considered the overall severity score of the 1702–1703 drought as a benchmark (with the lowest overall severity score) to estimate the likelihood (number of megadroughts/total number of years) CESM-LME during 850–2005. The likelihood was estimated using the number of megadroughts divided by the total number of years. We first estimated the number of megadroughts in all the ensemble members of CESM-LME (12×1156), divided by the number of years. The likelihood of such (~1702–1703) megadroughts (affected area more than 40% and PDSI less than -1.5) during the summer monsoon (JJA) in two consecutive years is less than one (~0.73) event in 100 years. On the other hand, the likelihood of the megadroughts like 2002–2003 is even lesser (~0.34 events in 100 years). Long-term PDSI from the CESM-LME for 1156 years (850–2005) from each ensemble member enables us to estimate the likelihood of megadroughts with a low probability of occurrence.

The composite MCA patterns of coupled variability between the summer monsoon precipitation and SST from all 12 ensemble members of CESM-LME show a negative relationship between summer monsoon rainfall and SST over the Pacific Ocean (Fig. 5a, b). The relationship exhibits clear patterns associated with the ENSO signature in CESM-LME simulations during the weak summer monsoon, consistent with the observed period (Fig. 4). To further confirm the role of SST variability over the Pacific Ocean, we constructed atmospheric and oceanic anomaly composites for all the megadroughts that occurred during the two consecutive years in CESM-LME (Fig. 5c, Supplementary Fig. 6). A total of 101 megadroughts of 2 successive years were identified in all the 12 ensemble members of CESM-LME. Consistent with the observed megadroughts (Fig. 4), the positive SST anomaly over the Pacific Ocean is strongly associated with the consecutive 2-year megadrought during the summer monsoon

season in CESM-LME (Fig. 5d). A majority (~60%) of megadroughts (61 out of 101) were associated with El Nino, positive IOD, and negative phase of PDO during the last millennium based on the CESM-LME simulations (Fig. 6a), which is consistent with the SST anomalies present during the observed megadrought of 2002–2003. Out of 61 megadroughts that were associated with El Nino during the last millennium, around 70% were also linked with positive DMI, negative PDO, and positive AMO (Fig. 6c). Analysis of climatological mean total precipitable water (TMQ) and wind field at 850 hPa showed the presence of higher TMQ over the tropical region and strong westerly wind flow during the summer monsoon (JJA) [Supplementary Fig. 6a]. Anomaly composite of TMQ and tropospheric winds showed dry TMQ anomalies and weaker westerly winds during the megadroughts of the two consecutive years (Supplementary Fig. 6b). The anomalous anticyclonic pattern observed for the megadroughts in CESM-LME is consistent with the observational analysis based on ERAS reanalysis (Supplementary Figs. 5 and 6). Similar climatological and anomalous patterns of TMQ and wind at 850 hPa were obtained for the megadroughts that occurred for the 3 consecutive years (Supplementary Fig. 6c). Megadroughts were widespread, with a mean coverage area of about 72%. Only two (1431–1433 and 1721–1723) megadroughts based on MADA-PDSI occurred for the 3 consecutive years (Supplementary Table 1). We considered the overall severity score (~311) of the 1431–1433 drought as a benchmark (the lowest severity score) to estimate the likelihood using CESM-LME. The probability of the three consecutive years megadroughts during the summer monsoon season is about 0.3 events per 100 years based on CESM-LME. Consistent with the megadroughts of two successive years, the role of positive SST anomalies on 3 consecutive years megadroughts over India was also exhibited (Supplementary Fig. 6c).

Like CESM-LME, CESM-Large Ensemble (CESM-LE hereafter) also captures the summer monsoon rainfall variability reasonably well during the historical climate^{59,66}. We used CESM-LE simulations from 40 different ensemble members for the 2021–2100 period to estimate the likelihood of megadroughts in the future climate. We calculated PDSI for each ensemble member of CESM-LE to identify megadroughts and their characteristics (Fig. 7a, b). The likelihood

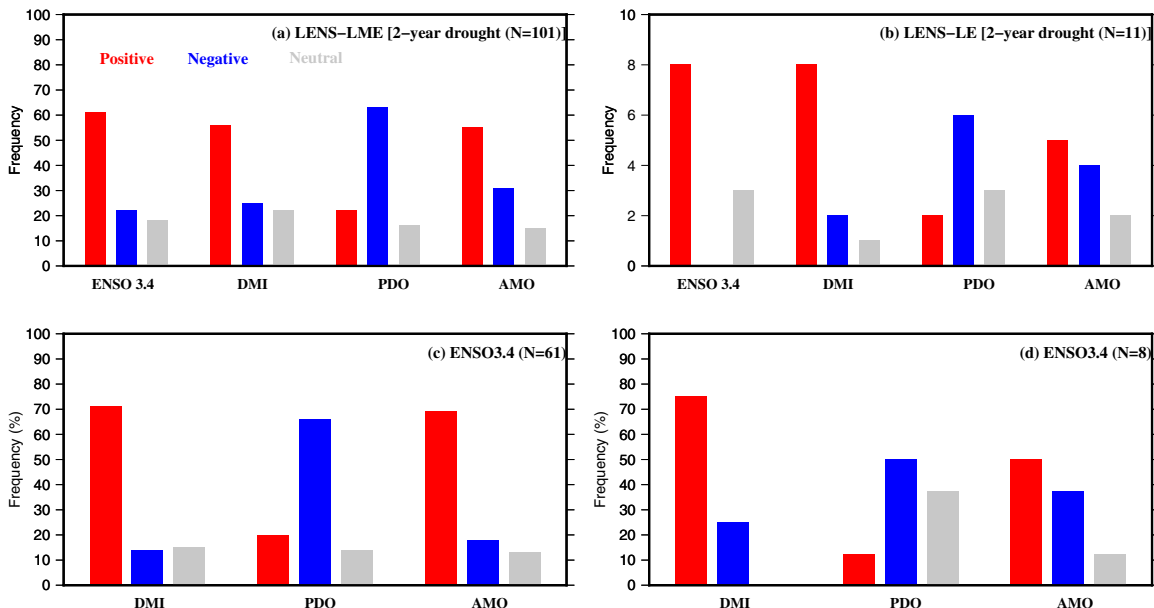


Fig. 6 The role of oceanic indices in historical and future megadroughts. a, b Megadrought frequency associated with ENSO3.4, DMI, PDO, and AMO during last millennium and future climate. **c, d** Co-occurrence of DMI, AMO, and PDO with ENSO3.4 associated megadroughts during last millennium and future climate, respectively. Positive and negative standardized anomalies of the oceanic indices were estimated using the threshold of 0.25 while neutral anomalies were considered if the values fell between -0.25 and 0.25 .

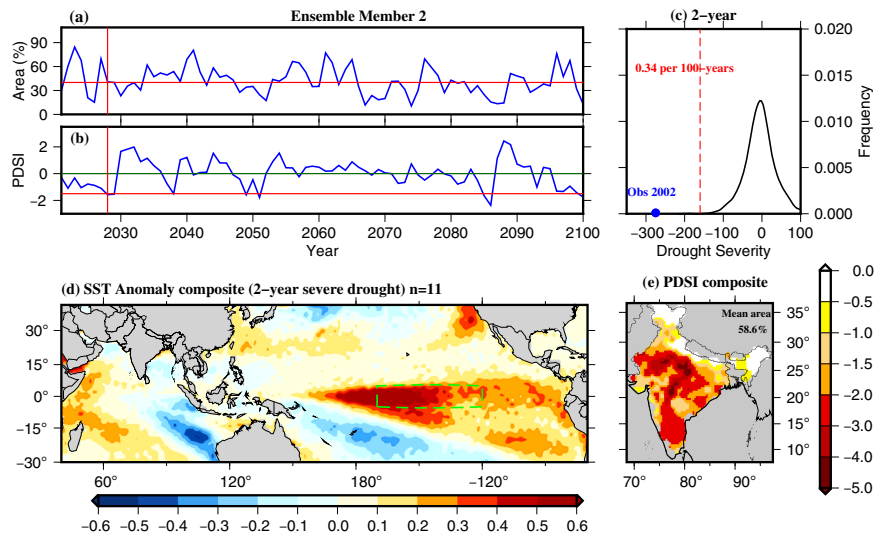


Fig. 7 Projected occurrence of megadroughts of two consecutive years in the future climate based on Community Earth System Model-Large Ensemble (CESM-LE). **a** Area under drought estimated using PDSI less than -1.5 using the ensemble member two of CESM-LE, **b** PDSI estimated using the ensemble member two of the CESM-LE, **c** kernel density function of drought severity estimated using all the 40 ensemble members of CESM-LE. The vertical red line in **c** indicates the minimum drought severity of the megadroughts of 2 consecutive years, while the blue circle shows the drought severity of the 2002 megadrought. **d** SST anomaly composite for the June to August period for all the consecutive 2-year droughts that had PDSI less than -1.5 and area under drought more than 40% (total 11 events in all the 40 ensemble members of 2021–2100 period each), and **e** composite of PDSI for all the megadroughts that occurred in all the 40 ensemble members of CESM-LE.

of megadroughts for 2 consecutive years is about 0.34 events per 100 years in the future, considering the threshold of the 1702–1703 drought estimated using MADA-PDSI. The composite analysis of all the megadroughts that occurred for the two consecutive years in CESM-LE showed the linkage of droughts with positive SST anomalies over the Pacific in the future climate (Fig. 7d, e and Supplementary Fig. 7), which is consistent with observations and CESM-LME simulations. We find that the future megadroughts during the summer monsoon over India will also be associated with El Nino, positive IOD, and negative phase of

PDO (Fig. 6c, d). Moreover, the climatological and anomaly patterns of total precipitable water and wind at 850 hPa showed dry anomalies for TMQ and weaker westerly flow during the megadroughts that are projected to occur in the future (Supplementary Fig. 7). However, we note that the TMQ anomalies are much stronger for the projected future climate than for the last millennium, attributable to the rising trend in total precipitable water under the warming climate (Supplementary Fig. 7). The likelihood of the megadroughts during the summer monsoon declines in the future (Fig. 7), which can be attributed to

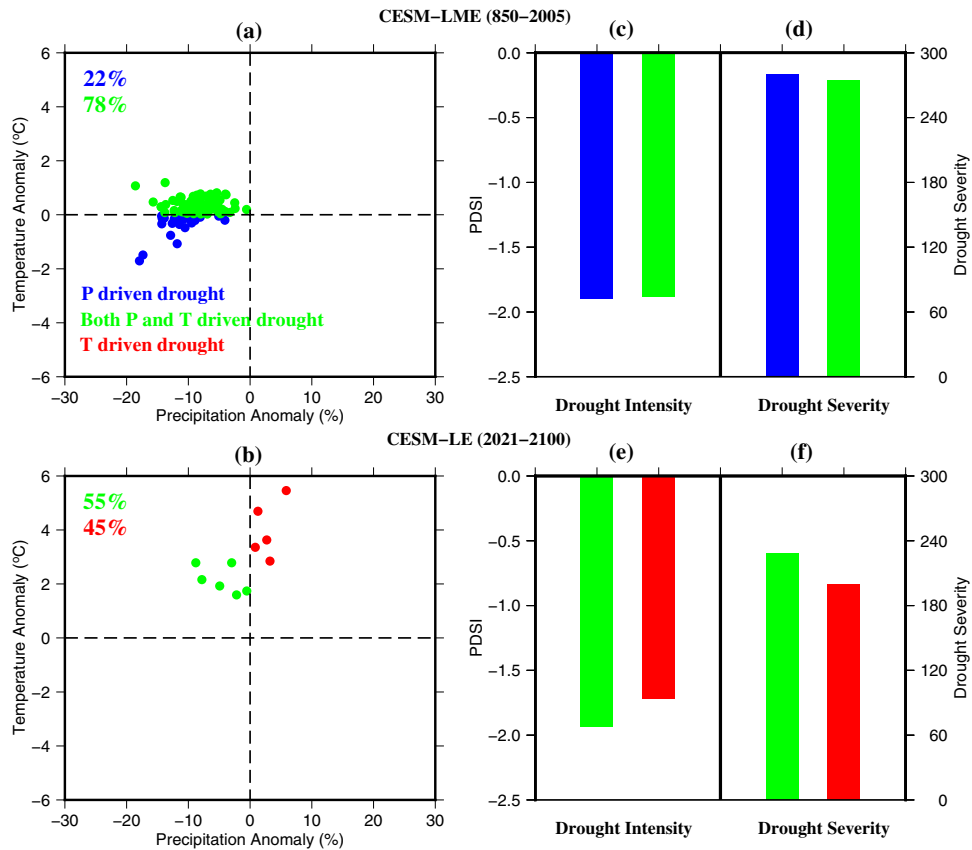


Fig. 8 Influence of temperature on the occurrence of 2-year consecutive megadroughts in the past (850–2005) and future climate (2021–2100). Precipitation and temperature anomaly during megadroughts of 2 consecutive years **a** in the last millennium (850–2005, CESM-LME) and **b** future climate (2021–2100, CESM-LE) based on Community Earth System Model. Anomalies of precipitation and temperature during the summer monsoon season were estimated against the reference period of 1951–2000. **c–f** Ensemble mean of drought severity and intensity during megadroughts of 2 consecutive years for each category [P-driven drought (blue); T-driven drought (red); and both P- and T-driven droughts] in **(c, d)** the last millennium (850–2005, CESM-LME) and **(e, f)** future climate (2021–2100, CESM-LE).

an increase in the summer monsoon precipitation under the warming climate⁶⁶. Moreover, MADA-PDSI is based on the June–August period, which does not consider the summer monsoon's variability during the late season. For instance, a considerable decline in India's summer monsoon season precipitation is reported during the late monsoon season in CESM-LE⁵⁹, affecting the severity and frequency of droughts in India.

Influence of climate warming on megadroughts

Droughts during the summer monsoon are mainly driven by the precipitation deficit, which can be exacerbated by warming^{7,66}. We examined the fraction of droughts caused by precipitation deficit, warming, and both by precipitation deficit and warming using the CESM-LME and CESM-LE simulations during the past and future climate, respectively (Fig. 8). We estimated the precipitation and temperature anomalies for all the megadroughts that occurred for two consecutive years for each ensemble member of CESM-LME and CESM-LE to identify the role of temperature in the droughts in the past and future. Droughts with precipitation deficits (negative precipitation anomaly) and negative temperature anomalies were considered precipitation deficit droughts (Fig. 8). During the summer monsoon and positive temperature anomalies, drought with precipitation deficits were considered precipitation deficits and temperature-driven droughts. On the other hand, droughts with no precipitation deficit and positive temperature anomaly were identified as temperature-driven droughts. Since precipitation and temperature anomalies during

the summer monsoon are negatively correlated⁶⁶, precipitation deficit can cause warming due to land-atmospheric feedback^{59,65,67,68}. However, we did not quantify the role of land-atmospheric coupling on warming and its impact on drought. Therefore, precipitation deficit and temperature-driven droughts may be more dominated by precipitation anomalies during the historical climate. Anomalies of precipitation and temperature during the summer monsoon season were estimated against the reference of 1951–2000 for both CESM-LME and CESM-LE simulations.

In the last millennium (CESM-LME), the megadroughts were driven by either only precipitation deficit or a combination of precipitation deficit and warm temperature (Fig. 8a). For instance, a majority (~78%) of megadroughts during the last millennium were caused by both precipitation deficit and warming during the summer monsoon. Around 22% of the total megadroughts in the last millennium were caused by precipitation deficit only during the summer monsoon season (Fig. 8a). However, megadroughts in the future are likely to be caused either by precipitation deficit and warming or solely due to a substantial rise in temperature (Fig. 8b). For instance, about 55% of future megadroughts are projected to be driven by both precipitation deficit and warming, while 45% of future megadroughts is driven only by due to rising in temperature (Fig. 8b). The substantial rise in air temperature and near-normal summer monsoon precipitation can also cause drought due to higher evapotranspiration⁶⁹ and increased atmospheric water demands. Moreover, only precipitation deficit megadroughts and a combination of precipitation deficit and

warm temperature megadroughts showed similar drought severity and intensity during the last millennium (Fig. 8c, d). However, precipitation deficit and warm temperature-driven megadroughts are projected to be more severe and intense than temperature-driven megadroughts under the projected future climate (Fig. 8e, f). Overall, we find that the likelihood of megadroughts consecutively for two years during the monsoon season is relatively low in future climate, which can be influenced by the significant warming that is projected. Therefore, the occurrence of megadroughts cannot be neglected under the warming climate.

DISCUSSION

Summer monsoon rainfall is critical for the food and water security of the large population in India. Understanding the drivers and likelihood of megadroughts is essential for the future food and water security of one of the world's most populated regions. However, the short instrumental record of the Indian summer monsoon underestimates the magnitude of rainfall variability³⁷. Recently gridded rainfall and temperature observations were extended to 1870, which were used to reconstruct the soil moisture droughts during the famines of the British Era⁹. We used long-term paleoclimate reconstructions for monsoon Asia, simulations from the CESM ensembles for the last millennium, and projected future climate to examine drivers of the megadroughts. As MADA-PDSI is based on paleoclimate reconstructions, we considered the widespread and severe droughts in our analysis. We found that the reported famines due to monsoon failures were well captured in MADA-PDSI.

Failure of the summer monsoon for consecutive years has detrimental implications for water availability, groundwater recharge, and food security. Recent droughts that occurred for the two successive years (2014–2015) in north India and South India (2016–2018) had lasting implications^{8,56}. We used a long-term PDSI based on MADA and CRU for the 1200–2018 period to identify the megadroughts that occurred for the two and three consecutive years. The likelihood of megadroughts for 2 and 3 successive years during the monsoon season is about 0.5 and 0.25 events per 100 years based on MADA-PDSI for 1200–2018. However, the likelihood of megadroughts was slightly increased in the longer-term record from the CESM-LME simulations. For instance, we find that the likelihood of 2- and 3-years megadroughts are about 0.73 and 0.3 events per 100 years in CESM-LME. The likelihood of 2- and 3-year megadroughts is projected to decline in the future climate, attributed to an increase in summer monsoon precipitation^{66,70}.

Summer monsoon failure and droughts played a vital role during the six significant famines captured using the MADA-PDSI. While most droughts in the past were caused due to the combination of precipitation deficit and warming, substantial warming that is projected in the future can cause droughts with near-normal precipitation during the summer monsoon. Given the dependence of a large population on agriculture and depletion of groundwater in several parts of the country^{71,72}, the occurrence of megadroughts in the future can have large implications despite its lower likelihood. While the megadroughts in the past caused food insecurity and famines in India⁹, famines are unlikely in the future despite the occurrence of megadroughts. India has made tremendous progress in improving crop yields due to enhanced agricultural practices and irrigation. Moreover, there has been a considerable growth in transportation and public distribution systems in the post-independence in India. For instance, despite the several intense and widespread droughts after the independence in India, the country did not experience famines⁹. The projected warming can result in a decline in the crop yields^{73,74}, which the hot and dry extremes⁶⁶ can further worsen. However, the risk of famines in the future remains low due to flood storage,

irrigation, public distribution system, rural employment, and transportation network^{75,76}.

Based on our findings, we conclude the following:

- Based on the long-term PDSI, six megadroughts were identified that occurred consecutively for 2 or 3 years during 1200–2018. Out of these six, four megadroughts lasted for 2 consecutive years and occurred during 1256–1257, 1423–1424, 1702–1703, and 2002–2003. Only two (1431–1433 and 1721–1723) megadroughts lasted for 3 consecutive years.
- We identified nine major famines caused by droughts during 1344–1345, 1630–1632, 1702–1704, 1769–1771, 1802–1804, 1837–1838, 1866, 1877, and 1899–1900.
- Based on CESM-LME simulations, the likelihood of 2 and 3-year consecutive megadroughts during the summer monsoon is about 0.7 and 0.3 events per 100 years, respectively. A majority of the past and future megadroughts are linked with El Nino. The frequency of megadroughts in the future is projected to decline due to increased monsoon season precipitation. However, substantial warming that is projected can influence the future megadroughts in India, which will have implications for food and water security.

METHODS

Observed data (1200–2018)

We used the combined long-term Monsoon Asia Drought Atlas (MADA³⁵) data for the past millennium (1200–2012) and recent Climate Research Unit (CRU) data for the period 2013–2018 to examine the occurrence of the consecutive megadroughts during 1200–2018. The last millennium MADA data was derived using the tree-ring chronologies of more than 300 sites across the forested areas of Monsoon Asia³⁵ to reconstruct the Palmer Drought Severity Index (PDSI)⁷⁷ for the summer monsoon season (June–August). The reconstructed PDSI from MADA (hereafter MADA-PDSI) is available for 534 grid points of Monsoon Asia at 1° spatial resolution for 1200–2012, which was developed using a correlation-weighted and ensemble-based modification of point-by-point regression (PPR) method^{35,78}. Using the PPR method, a well-calibrated and validated dataset of PDSI was reconstructed³⁵. Previously, the PPR method was also used to produce a high-quality reconstruction of PDSI over North America [North American Drought Atlas⁷⁸]. Similarly, the reconstructed PDSI data over Monsoon Asia was calibrated and validated against the observed global PDSI data from Dai et al.⁷⁹ for 1870–2002. The global PDSI of Dai et al.⁷⁹ (Dai-PDSI) was developed using the precipitation and temperature from the CRU. Therefore, we used the PDSI from the CRU (<https://crudata.uea.ac.uk/cru/data/drought/>) at 0.5° spatial resolution for 1901–2018^{80,81}, which was further regridded at 1° spatial resolution to validate the MADA-PDSI data. Using PDSI (MADA-PDSI from 1200–2012 and CRU-PDSI from 2013–2018), we evaluated the summer monsoon drought severity and occurrence over India for 1200–2018.

We used observed precipitation and sea surface temperature (SST) for the period 1901–2018. The monthly gridded precipitation was obtained from CRU (version 4.03⁵⁷) for 1901–2018 at 0.5° spatial resolution over India. CRU-precipitation is developed using many observed datasets using the angular-distance weighting interpolation at a monthly time scale⁵⁷. Gridded products from the CRU have been widely used for regional and global drought and hydroclimatic extreme studies^{82,83}.

We obtained monthly SST from the Hadley Centre's (HadSST, <https://www.metoffice.gov.uk/hadobs/hadisst/>) from 1901 to 2018 to evaluate the linkage between drought (PDSI and precipitation anomalies) and SST⁸⁴. The HadSST data were reconstructed using the two-stage reduced-space optimal interpolation of observation data at 1° spatial resolution⁸⁴. We estimated oceanic indices, including the ENSO, DMI, AMO, and PDO using HadSST for the observed period. ENSO was estimated using the area-weighted average SST anomalies over the Niño 3.4 region (5°N–5°S, 120–170°W; Supplementary Fig. 8). Indian Summer Monsoon droughts are highly correlated with the SST anomalies over the Niño-3.4 region compared to the other Niño regions⁷. DMI was calculated using the difference between the area-averaged SST anomalies of western (10°S–10°N, 50°E–70°E; Supplementary Fig. 8) and eastern (10°S–0°N, 90°E–110°E) Indian Ocean regions⁸⁵. Similarly, area-averaged SST anomaly in the North

Atlantic region (0°N - 60°N , 0 - 80°W ; Supplementary Fig. 8) represents the AMO^{86,87} while PDO was estimated using the leading pattern of SST anomalies over Northern Pacific Ocean (north of 20°N)^{27,88}. We used EOF analysis to identify the leading principle component over the Northern Pacific Ocean (20°N - 60°N , 120°E - 100°W ; Supplementary Fig. 8), which was used for estimating PDO. Moreover, we obtained TCRW, and wind (u and v components) at 850hPa from the European Centre for Medium-Range Weather Forecasts Reanalysis version 5 (ERA-5⁸⁹) for the period 1979–2018 to evaluate available moisture content and atmospheric condition during observed megadroughts.

Data from CESM

Community Earth System Model realistically simulates the coupling between ISMR and SST variability over the Pacific Ocean⁶⁶. Moreover, CESM-1 simulations reproduce seasonality and spatial variability in summer monsoon rainfall reasonably well⁴⁶. Most global climate models show bias in summer monsoon precipitation and do not capture the ENSO-monsoon coupling well^{70,90}. We, therefore, selected the CESM-1 for the present work. Moreover, simulations from many ensemble members are available for the past, present, and future periods, making CESM suitable for the analysis to estimate the likelihood of megadroughts in India. We used simulations from the CESM-LME⁹¹ project (<https://www.cesm.ucar.edu/projects/community-projects/LME/>) to evaluate the likelihood of the occurrence of the consecutive droughts over India during the period 850–2005. We used 12 runs (out of 13; the first run does not have the data for the entire period of 850–2005) of CESM-LME for the 850–2005 period to estimate monthly PDSI. Monthly precipitation, surface air temperature (maximum and minimum), specific humidity, wind speed, latent heat flux, sensible heat flux, and surface pressure were used to estimate India's PDSI. PDSI was calculated using precipitation, atmospheric water demand (potential evapotranspiration: PET), and available water content (AWC) of soil⁹². Atmospheric water demand (PET) was estimated using the Penman-Monteith method^{93,94}, while AWC was obtained from the Harmonized World Soil Database (HWSD⁹⁵). We analyzed the consecutive droughts and their characteristics over India in the last millennium using PDSI from the 12 ensemble members from CESM-LME.

We used data from the 40 ensemble members from the Community Earth System Model- Large Ensemble (CESM-LE⁹⁶) project (<http://www.cesm.ucar.edu/projects/community-projects/LENS/>) for the period 2021–2100 to examine the drought occurrence in the future climate. We estimated the atmospheric water demand (PET) using the modified Penman-Monteith method⁹⁷ for the future (2021–2100) using monthly surface air temperature, wind speed, specific humidity, surface pressure, and latent and sensible heat flux. We used the modified Penman-Monteith method since the changes in surface resistance due to the increased warming climate were not considered in the Penman-Monteith method, affecting the drought severity in the future climate⁶⁹. Using the PET, precipitation, and AWC, we estimated PDSI for 2021–2100 using the 40 runs of CESM-LE to understand the future drought severity. The CESM-LE simulations have been widely used to analyze drought and extreme climate studies under the future climate^{66,69,98}. We used monthly SST, total precipitable water (TMQ), and wind at 850hPa from CESM-LME and CESM-LE for 850–2005 and 2021–2100, respectively. As SST and TMQ from CESM-LE for the future period (2021–2100) has a strong warming trend, we used Ensemble Empirical Mode Decomposition (EEMD⁹⁹) to remove secular trend¹⁰⁰ from TMQ and SST for the period 2021–2100. Moreover, we examined the year-to-year variability between the summer monsoon (JJA) precipitation and SST¹³. The MCA⁵⁸ method was used to evaluate the coupled variability between precipitation and SST. We identify the first leading mode of variation between rainfall and temperature using the MCA, which shows the substantial coupled variability between two fields (precipitation and SST). Similar to observation, we estimated oceanic indices including ENSO (Niño 3.4), DMI, AMO, and PDO from CESM-LME and CESM-LE simulations for the past and future climate. Moreover, TMQ and wind at 850hPa were used to evaluate available moisture content and atmospheric condition during megadroughts in LENS-LME and LENS-LE.

DATA AVAILABILITY

All the datasets used in this study can be obtained from the corresponding author.

CODE AVAILABILITY

Data processing scripts can be obtained from the corresponding author.

Received: 5 May 2021; Accepted: 5 November 2021;

Published online: 01 December 2021

REFERENCES

- Kumar, K. N., Rajeevan, M., Pai, D. S., Srivastava, A. K. & Preethi, B. On the observed variability of monsoon droughts over India. *Weather Clim. Extrem.* **1**, 42–50 (2013).
- Gadgil, S. & Gadgil, S. The Indian monsoon, GDP and agriculture. *Econ. Polit. Wkly.* **41**, 4887–4895 (2006).
- Gadgil, S. & Kumar, K. R. The Asian monsoon—agriculture and economy. in *The Asian Monsoon* 651–683 (Springer, Berlin, Heidelberg, 2006).
- Gadgil, S., Vinayachandran, P. N. & Francis, P. A. Droughts of the Indian summer monsoon: role of clouds over the Indian Ocean. *Curr. Sci.* **85**, 1713–1719 (2003).
- Sikka, D. R. *Monsoon Drought in India*. (1999).
- Shah, D. & Mishra, V. Drought onset and termination in India. *J. Geophys. Res. Atmos.* **125**, e2020JD032871 (2020).
- Mishra, V. Long-term (1870–2018) drought reconstruction in context of surface water security in India. *J. Hydrol.* **580**, 124228 (2020).
- Mishra, V., Aadhar, S., Asoka, A., Pai, S. & Kumar, R. On the frequency of the 2015 monsoon season drought in the Indo-Gangetic Plain. *Geophys. Res. Lett.* **43**, 12,102–12,112 (2016).
- Mishra, V. et al. Drought and Famine in India, 1870–2016. *Geophys. Res. Lett.* **46**, 2075–2083 (2019).
- Singh, D. et al. Climate and the Global Famine of 1876–78. *J. Clim.* **31**, 9445–9467 (2018).
- Kumar, K. K., Rajagopalan, B. & Cane, M. A. On the weakening relationship between the Indian monsoon and ENSO. *Science* **284**, 2156–2159 (1999).
- Ashok, K., Guan, Z., Saji, N. H. & Yamagata, T. Individual and combined influences of ENSO and the Indian Ocean Dipole on the Indian summer monsoon. *J. Clim.* **17**, 3141–3155 (2004).
- Mishra, V., Smoliak, B. V., Lettenmaier, D. P. & Wallace, J. M. A prominent pattern of year-to-year variability in Indian Summer Monsoon Rainfall. *Proc. Natl Acad. Sci. USA* **109**, 7213–7217 (2012).
- Singh, D., Ghosh, S., Roxy, M. K. & McDermid, S. Indian summer monsoon: extreme events, historical changes, and role of anthropogenic forcings. *WIREs Clim. Chang.* **10**, e571 (2019).
- Kirtman, B. P. & Shukla, J. Influence of the Indian summer monsoon on ENSO. *Q. J. R. Meteorol. Soc.* **126**, 213–239 (2000).
- Abid, M. A., Almazroui, M., Kucharski, F., O'Brien, E. & Yousef, A. E. ENSO relationship to summer rainfall variability and its potential predictability over Arabian Peninsula region. *npj Clim. Atmos. Sci.* **1**, 1–7 (2018).
- Kucharski, F. & Abid, M. A. Interannual Variability of the Indian Monsoon and Its Link to ENSO. *Oxford Res. Encycl. Clim. Sci.* <https://doi.org/10.1093/ACREFORE/9780190228620.013.615> (2017).
- Ashok, K., Guan, Z. & Yamagata, T. Influence of the Indian Ocean Dipole on the Australian winter rainfall. *Geophys. Res. Lett.* **30**, 1821 (2003).
- Cai, W., Cowan, T. & Sullivan, A. Recent unprecedented skewness towards positive Indian Ocean Dipole occurrences and its impact on Australian rainfall. *Geophys. Res. Lett.* **36** (2009).
- Saji, N. H., Goswami, B. N., Vinayachandran, P. N. & Yamagata, T. A dipole mode in the tropical Indian ocean. *Nature* **401**, 360–363 (1999).
- Saji, N. H. & Yamagata, T. Possible impacts of Indian Ocean Dipole mode events on global climate. *Clim. Res.* **25**, 151–169 (2003).
- Webster, P. J., Moore, A. M., Loschnigg, J. P. & Leben, R. R. Coupled ocean-atmosphere dynamics in the Indian Ocean during 1997–98. *Nature* **401**, 356–360 (1999).
- Ihara, C., Kushnir, Y., Cane, M. A. & De La Peña, V. H. Indian summer monsoon rainfall and its link with ENSO and Indian Ocean climate indices. *Int. J. Climatol.* **27**, 179–187 (2007).
- Schott, F. A., Xie, S. P. & McCreary, J. P. Indian ocean circulation and climate variability. *Rev. Geophys.* **47**, RG1002 (2009).
- Ummenhofer, C. C. et al. Multi-decadal modulation of the El Niño-Indian monsoon relationship by Indian Ocean variability. *Environ. Res. Lett.* **6**, 34006–34014 (2011).
- Ashok, K., Guan, Z. & Yamagata, T. Impact of the Indian Ocean dipole on the relationship between the Indian monsoon rainfall and ENSO. *Geophys. Res. Lett.* **28**, 4499–4502 (2001).
- Krishnamurthy, L. & Krishnamurthy, V. Influence of PDO on South Asian summer monsoon and monsoon-ENSO relation. *Clim. Dyn.* **42**, 2397–2410 (2014).
- Kucharski, F., Molteni, F. & Yoo, J. H. SST forcing of decadal Indian Monsoon rainfall variability. *Geophys. Res. Lett.* **33**, 3709 (2006).
- Goswami, B. N., Kripalani, R. H., Borgaonkar, H. P. & Preethi, B. Multi-decadal variability in Indian summer monsoon rainfall using proxy data. *World Sci. Ser. Asia Pac. Weather Clim.* **6**, 327–345 (2016).

30. Naidu, P. D. et al. Coherent response of the Indian Monsoon Rainfall to Atlantic multi-decadal variability over the last 2000 years. *Sci. Rep.* **10**, 1–11 (2020).
31. Walford, C. The famines of the world: past and present. *J. Stat. Soc. Lond.* **41**, 433 (1878).
32. Sen, A. Famines. *World Dev.* **8**, 613–621 (1980).
33. Bhalme, H. N. & Mooley, D. A. Large-scale droughts/ floods and monsoon circulation. *Mon. Weather Rev.* **108**, 1197–1211 (1980).
34. Devereux, S. Famine in the twentieth century. *IDS Work. Pap.* **105** **1**, 40 (2000).
35. Cook, E. R. et al. Asian monsoon failure and megadrought during the last millennium. *Science* **328**, 486–489 (2010).
36. Cook, E. R. et al. Old World megadroughts and pluvials during the Common Era. *Sci. Adv.* **1**, 37 (2015).
37. Sinha, A. et al. A 900-year (600 to 1500 A.D.) record of the Indian summer monsoon precipitation from the core monsoon zone of India. *Geophys. Res. Lett.* **34**, L16707 (2007).
38. Brázdil, R. et al. Central Europe, 1531–1540 CE: the driest summer decade of the past five centuries? *Climate* **16**, 2125–2151 (2020).
39. Lin, K.-H. E., Wang, P. K., Pai, P.-L., Lin, Y.-S. & Wang, C.-W. Historical droughts in the Qing dynasty (1644–1911) of China. *Climate* **16**, 911–931 (2020).
40. Sinha, A. et al. Trends and oscillations in the Indian summer monsoon rainfall over the last two millennia. *Nat. Commun.* **6**, 6309 (2015).
41. Mishra, V., Aadhar, S., Asoka, A., Pai, S. & Kumar, R. On the frequency of the 2015 monsoon season drought in the Indo-Gangetic Plain. *Geophys. Res. Lett.* **43**, 12,102–12,112 (2016).
42. Nguyen, H. T. T., Turner, S. W. D., Buckley, B. M. & Galelli, S. Coherent streamflow variability in monsoon Asia over the past eight centuries—links to oceanic drivers. *Water Resour. Res.* **56**, e2020WR027883 (2020).
43. Yang, B. et al. Drought variability at the northern fringe of the Asian summer monsoon region over the past millennia. *Clim. Dyn.* **43**, 845–859 (2014).
44. Mujumdar, M., Kumar, V. & Krishnan, R. The Indian summer monsoon drought of 2002 and its linkage with tropical convective activity over northwest Pacific. *Clim. Dyn.* **28**, 743–758 (2007).
45. Bhat, G. S. The Indian drought of 2002—a sub-seasonal phenomenon? *Q. J. R. Meteorol. Soc.* **132**, 2583–2602 (2006).
46. Ummenhofer, C. C., D'Arrigo, R. D., Anchukaitis, K. J., Buckley, B. M. & Cook, E. R. Links between Indo-Pacific climate variability and drought in the Monsoon Asia Drought Atlas. *Clim. Dyn.* **40**, 1319–1334 (2013).
47. Fieldhouse, P. Community shared agriculture. *Agric. Hum. Values* **13**, 43–47 (1996).
48. Butler, S. H. Famine. in *The Imperial Gazetteer of India Vol. III* (Clarendon Press, Oxford, 1908).
49. Wilson, I. R. G. Can we predict the next Indian mega-famine? *Energy Environ.* **20**, 11–24 (2009).
50. Gráda, C. Ó. Making famine history. *J. Econ. Lit.* **45**, 5–38 (2007).
51. Attwood, D. W. Big is ugly? How large-scale institutions prevent famines in Western India. *World Dev.* **33**, 2067–2083 (2005).
52. Winters, R., Hume, J. P. & Leenstra, M. A famine in Surat in 1631 and Dodos on Mauritius: a long lost manuscript rediscovered. *Arch. Nat. Hist.* **44**, 134–150 (2017).
53. Sen, A. Ingredients of famine analysis: availability and entitlements. *Q. J. Econ.* **96**, 433 (1981).
54. Jonsson, F. A. *Enlightenment's Frontier*. (Yale University Press, London, 2013).
55. Patel, D. Viewpoint: How British let one million Indians die in famine. *BBC NEWS* (2016).
56. Mishra, V., Thirumalai, K., Jain, S. & Aadhar, S. Unprecedented drought in South India and recent water scarcity. *Environ. Res. Lett.* **16**, 054007 (2021).
57. Harris, I., Osborn, T. J., Jones, P. & Lister, D. Version 4 of the CRU TS monthly high-resolution gridded multivariate climate dataset. *Sci. Data* **7**, 1–18 (2020).
58. Bretherton, C. S., Smith, C. & Wallace, J. M. An intercomparison of methods for finding coupled patterns in climate data. *J. Clim.* **5**, 541–560 (1992).
59. Mishra, V., Aadhar, S. & Mahto, S. S. Anthropogenic warming and intraseasonal summer monsoon variability amplify the risk of future flash droughts in India. *npj Clim. Atmos. Sci.* **4**, 1–10 (2021).
60. Kumar, K. K., Rajagopalan, B., Hoerling, M., Bates, G. & Cane, M. Unraveling the mystery of Indian monsoon failure during El Niño. *Science* **314**, 115–119 (2006).
61. Roxy, M. K. et al. Drying of Indian subcontinent by rapid Indian Ocean warming and a weakening land-sea thermal gradient. *Nat. Commun.* **6**, 7423 (2015).
62. Yadav, R. K. & Roxy, M. K. On the relationship between north India summer monsoon rainfall and east equatorial Indian Ocean warming. *Glob. Planet. Change* **179**, 23–32 (2019).
63. Krishnamurthy, L. & Krishnamurthy, V. Teleconnections of Indian monsoon rainfall with AMO and Atlantic tripole. *Clim. Dyn.* **46**, 2269–2285 (2016).
64. Bhat, G. S. The Indian drought of 2002—a sub-seasonal phenomenon? *Q. J. R. Meteorol. Soc.* **132**, 2583–2602 (2006).
65. Berg, A. et al. Land-atmosphere feedbacks amplify aridity increase over land under global warming. *Nat. Clim. Chang.* **6**, 869–874 (2016).
66. Mishra, V., Thirumalai, K., Singh, D. & Aadhar, S. Future exacerbation of hot and dry summer monsoon extremes in India. *npj Clim. Atmos. Sci.* **3**, 10 (2020).
67. Zhou, S. et al. Land-atmosphere feedbacks exacerbate concurrent soil drought and atmospheric aridity. *Proc. Natl. Acad. Sci. USA* **116**, 18848–18853 (2019).
68. Dirmeyer, P. A., Balsamo, G., Blyth, E. M., Morrison, R. & Cooper, H. M. Land-atmosphere interactions exacerbated the drought and heatwave over Northern Europe during summer 2018. *AGU Adv.* **2**, e2020AV000283 (2021).
69. Aadhar, S. & Mishra, V. Increased drought risk in South Asia under warming climate: implications of uncertainty in potential evapotranspiration estimates. *J. Hydrometeorol.* **21**, 2979–2996 (2020).
70. Menon, A., Levermann, A., Schewe, J., Lehmann, J. & Frieler, K. Consistent increase in Indian monsoon rainfall and its variability across CMIP-5 models. *Earth Syst. Dyn.* **4**, 287–300 (2013).
71. Asoka, A., Gleeson, T., Wada, Y. & Mishra, V. Relative contribution of monsoon precipitation and pumping to changes in groundwater storage in India. *Nat. Geosci.* **10**, 109–117 (2017).
72. Asoka, A., Wada, Y., Fishman, R. & Mishra, V. Strong linkage between precipitation intensity and monsoon season groundwater recharge in India. *Geophys. Res. Lett.* **45**, 5536–5544 (2018).
73. Zhao, C. et al. Plausible rice yield losses under future climate warming. *Nat. Plants* **3**, 1–5 (2016).
74. Tigchelaar, M., Battisti, D. S., Naylor, R. L. & Ray, D. K. Future warming increases probability of globally synchronized maize production shocks. *Proc. Natl. Acad. Sci. USA* **115**, 6644–6649 (2018).
75. Gráda, C. O. Famine is not the problem: a historical perspective. *Hist. Res.* **88**, 20–33 (2015).
76. Gráda, C. Ó. Famines past, famine's future. *Dev. Change* **42**, 49–69 (2011).
77. Wells, N., Goddard, S. & Hayes, M. J. A self-calibrating Palmer drought severity index. *J. Clim.* **17**, 2335–2351 (2004).
78. Cook, E. R., Seager, R., Cane, M. A. & Stahle, D. W. North American drought: reconstructions, causes, and consequences. *Earth* **81**, 93–134 (2007).
79. Dai, A., Trenberth, K. E. & Qian, T. A global dataset of Palmer Drought Severity Index for 1870–2002: relationship with soil moisture and effects of surface warming. *J. Hydrometeorol.* **5**, 1117–1130 (2004).
80. Van Der Schrier, G., Barichivich, J., Briffa, K. R. & Jones, P. D. A scPDSI-based global data set of dry and wet spells for 1901–2009. *J. Geophys. Res. Atmos.* **118**, 4025–4048 (2013).
81. Barichivich, J., Osborn, T., Harris, I., van der Schrier, G. & Jones, P. Drought monitoring global drought using the self-calibrating Palmer Drought Severity Index. *Bull. Am. Meteorol. Soc.* **100**, S39–S40 (2019).
82. Asadi Zarch, M. A., Sivakumar, B. & Sharma, A. Droughts in a warming climate: a global assessment of Standardized precipitation index (SPI) and Reconnaissance drought index (RDI). *J. Hydrol.* **526**, 183–195 (2015).
83. Aadhar, S. & Mishra, V. A substantial rise in the area and population affected by dryness in South Asia under 1.5 °C, 2.0 °C and 2.5 °C warmer worlds. *Environ. Res. Lett.* **14**, 114021 (2019).
84. Rayner, N. A. et al. Global analyses of sea surface temperature, sea ice, and night marine air temperature since the late nineteenth century. *J. Geophys. Res. D Atmos.* **108**, 4407 (2003).
85. Singh, D. et al. Climate and the global famine of 1876–78. *J. Clim.* **31**, 9445–9467 (2018).
86. Zhang, R. & Delworth, T. L. Impact of Atlantic multidecadal oscillations on India/Sahel rainfall and Atlantic hurricanes. *Geophys. Res. Lett.* **33**, L17712 (2006).
87. Enfield, D. B., Mestas-Nuñez, A. M. & Trimble, P. J. The Atlantic multidecadal oscillation and its relation to rainfall and river flows in the continental U.S. *Geophys. Res. Lett.* **28**, 2077–2080 (2001).
88. Mantua, N. J., Hare, S. R., Zhang, Y., Wallace, J. M. & Francis, R. C. A pacific interdecadal climate oscillation with impacts on salmon production. *Bull. Am. Meteorol. Soc.* **78**, 1069–1079 (1997).
89. Hersbach, H. & Dee, D. ERA5 reanalysis is in production. *ECMWF Newsl.* **147**, 5–6 (2016).
90. Ashfaq, M., Rastogi, D., Mei, R., Touma, D. & Leung, L. R. Sources of errors in the simulation of south Asian summer monsoon in the CMIP5 GCMs. *Clim. Dyn.* **49**, 193–223 (2017).
91. Otto-Bliesner, B. L. et al. Climate variability and change since 850 ce an ensemble approach with the community earth system model. *Bull. Am. Meteorol. Soc.* **97**, 787–801 (2016).
92. Palmer, W. C. Meteorological Drought. *U.S. Weather Bureau, Research Paper No. 45*, 58 (1965).
93. Penman, H. L. Natural evaporation from open water, bare soil and grass. *Proc. R. Soc. A Math. Phys. Eng. Sci.* **193**, 120–145 (1948).
94. Monteith, J. L. Evaporation and environment. in *19th Symposia of the Society for Experimental Biology* 19 205–234 (University Press, Cambridge, 1965).
95. Nachtergaelie, F. O. et al. The harmonized world soil database. in *Proc. 19th World Congress of Soil Science, Soil Solutions for a Changing World* 34–37 (2010).

96. Kay, J. E. et al. The Community Earth System Model (CESM) Large Ensemble Project: A Community Resource for Studying Climate Change in the Presence of Internal Climate Variability. *Bull. Am. Meteorol. Soc.* **96**, 1333–1349 (2015).
97. Yang, Y., Roderick, M. L., Zhang, S., McVicar, T. R. & Donohue, R. J. Hydrologic implications of vegetation response to elevated CO₂ in climate projections. *Nat. Clim. Chang.* **9**, 44–48 (2019).
98. Ault, T. R. On the essentials of drought in a changing climate. *Science* **368**, 256–260 (2020).
99. Wu, Z. & Huang, N. E. Ensemble empirical mode decomposition: a noise-assisted data analysis method. *Adv. Adapt. Data Anal.* **1**, 1–41 (2009).
100. Wu, Z., Huang, N. E., Wallace, J. M., Smoliak, B. V. & Chen, X. On the time-varying trend in global-mean surface temperature. *Clim. Dyn.* **37**, 759–773 (2011).

ACKNOWLEDGEMENTS

Authors acknowledge the data availability from Monsoon Asia Drought Atlas (MADA), Community Earth System Model's Last Millennium Ensemble (CESM-LME), and CESM Large Ensemble (CESM-LE). All the datasets are freely available. The financial assistance for this work was provided by the Ministry of Environment, Forest, and Climate Change (MoEFCC).

AUTHOR CONTRIBUTIONS

V.M. designed the study and wrote the paper. S.A. estimated PDSI and contributed to the analysis.

COMPETING INTERESTS

The authors declare no competing interests.

ADDITIONAL INFORMATION

Supplementary information The online version contains supplementary material available at <https://doi.org/10.1038/s41612-021-00219-1>.

Correspondence and requests for materials should be addressed to Vimal Mishra.

Reprints and permission information is available at <http://www.nature.com/reprints>

Publisher's note Springer Nature remains neutral with regard to jurisdictional claims in published maps and institutional affiliations.



Open Access This article is licensed under a Creative Commons Attribution 4.0 International License, which permits use, sharing, adaptation, distribution and reproduction in any medium or format, as long as you give appropriate credit to the original author(s) and the source, provide a link to the Creative Commons license, and indicate if changes were made. The images or other third party material in this article are included in the article's Creative Commons license, unless indicated otherwise in a credit line to the material. If material is not included in the article's Creative Commons license and your intended use is not permitted by statutory regulation or exceeds the permitted use, you will need to obtain permission directly from the copyright holder. To view a copy of this license, visit <http://creativecommons.org/licenses/by/4.0/>.

© The Author(s) 2021